J|A|C|S ARTICLES

Published on Web 11/03/2010

Factors Controlling the Mechanism of NAD$^+$ Non-Redox Reactions

Todor Dudev[†] and Carmay Lim*[,†,‡]

Institute of Biomedical Sciences, Academia Sinica, Taipei 115, Taiwan, and Department of Chemistry, National Tsing Hua University, Hsinchu 300, Taiwan

Received July 26, 2010; E-mail: carmay@gate.sinica.edu.tw

Abstract: β-Nicotinamide adenine dinucleotide (NAD$^+$) is an indispensable coenzyme or substrate for enzymes involved in catalyzing redox and non-redox reactions. ADP-ribosylating enzymes catalyze cleavage of the nicotinamide−glycosyl bond of NAD$^+$ and addition of a nucleophilic group from their substrate proteins to the *N*-ribose anomeric carbon of NAD$^+$. Although the role of the nicotinamide−ribose fragment in the mechanism of NAD$^+$ hydrolysis has been examined, the role of the doubly negatively charged, flexible, and chemically reactive NAD$^+$ diphosphate moiety in the reaction process has largely been neglected. Thus, the participation of the pyrophosphate group in stabilizing intra- and intermolecular interactions in the ground state and transition state has not been explored. Furthermore, the roles of other factors such as the type/nucleophilicity of the attacking nucleophile and the medium in influencing the reaction pathway have not been systematically evaluated. In this study, we endeavor to fill in these gaps and elucidate the role of these factors in controlling the NAD$^+$ nicotinamide−glycosyl bond cleavage. Using density functional theory combined with continuum dielectric methods, we modeled both S_N1 and S_N2 reaction pathways and assessed the role of the diphosphate group in stabilizing the (i) NAD$^+$ ground state, (ii) oxocarbocation intermediate, (iii) reaction product, and (iv) nucleophile. We also assessed the chemical nature of the attacking nucleophile and the role of the protein matrix in affecting the reaction mechanism. Our results reveal an intricate interplay among various factors in controlling the reaction pathway, which in turn suggests ways in which the enzyme can accelerate the reaction.

Introduction

β-Nicotinamide adenine dinucleotide (NAD$^+$; Figure 1A) is an indispensable coenzyme in all living cells where it participates in redox and non-redox reactions. In the latter, NAD$^+$ acts as a substrate for certain enzymes and undergoes chemical transformation: The bond between the *N*-ribose anomeric C* and the nicotinamide N^{1N} is cleaved, and a nucleophilic group (:Nu) from the attacking agent is attached to C* (see Schemes 1 and 2). The nucleophile can be water, cysteine, arginine, acetyl-lysine, or diphthamide, a posttranslationally modified histidine (Figure 1C). Enzymes catalyzing the C*−N^{1N} bond cleavage and subsequent ADP-ribose transfer to their target proteins include sirtuins,[1,2] poly(ADP-ribose)-polymerases,[3] and a group of deadly bacterial ADP-ribosylating toxins such as cholera, diphtheria, pertussis, and cholix.[4,5] Because poly(ADP-ribose)-polymerases are promising targets for drug development aimed at inflammation, degenerative and vascular diseases, ischemia, and cancer,[6−8] while ADP-ribosylating toxins serve as drug targets for treating infections by lethal bacteria,[9−15] it is of great interest to elucidate the mechanism of their common reaction and the factors controlling the reaction mechanism. Knowledge of the interactions stabilizing the rate-limiting transition state (TS) of the enzymatic reaction could be exploited in designing TS analogue inhibitors.

Although there are several studies on the nonenzymatic and enzyme-catalyzed hydrolysis of NAD$^+$, the exact mechanism of the process remains elusive and is still a subject of controversy. Both unimolecular (S_N1) and bimolecular (S_N2) mechanisms have been invoked, and they compete to explain the experimental and theoretical data. The S_N1 pathway stipulates a two-step reaction (Scheme 1): First, the C*−N^{1N} bond between the positively charged nicotinamide and the *N*-ribose of NAD$^+$ is cleaved, yielding a neutral nicotinamide and an oxocarbocation intermediate (ADP-ribose). Second, the

[†] Academia Sinica.
[‡] National Tsing Hua University.

(1) Blander, G.; Guarente, L. *Annu. Rev. Biochem.* **2004**, *73*, 417.
(2) Sauve, A. A.; Wolberger, C.; Schramm, V. L.; Boeke, J. D. *Annu. Rev. Biochem.* **2006**, *75*, 435.
(3) Pellicciari, R.; Camaioni, E.; Castantino, G. *Prog. Med. Chem.* **2004**, *42*, 125.
(4) Yates, S.; Jorgensen, R.; Andersen, G.; Merrill, A. *Trends Biochem. Sci.* **2006**, *31*, 123.
(5) Fieldhouse, R. J.; Merrill, A. R. *Trends Biochem. Sci.* **2008**, *33*, 546.
(6) Jagtap, P.; Szab, C. *Nat. Rev. Drug Discovery* **2005**, *4*, 421.
(7) Ratnam, K.; Low, J. A. *Clin. Cancer Res.* **2007**, *13*, 1383.
(8) Peralta-Leal, A.; Rodriguez-Vargas, J. M.; Aguilar-Quesada, R.; Rodriguez, M. I.; Linares, J. L.; de Almod var, M. R.; Oliver, F. J. *Free Radical Biol. Med.* **2009**, *47*, 13.
(9) Yates, S. P.; Merrill, A. R. *J. Biol. Chem.* **2001**, *276*, 35029.
(10) Roberts, T. M.; Merrill, A. R. *Biochem. J.* **2002**, *367*, 601.
(11) Armstrong, S.; Merrill, A. R. *Biochemistry* **2004**, *43*, 183.
(12) Parikh, S.; Schramm, V. *Biochemistry* **2004**, *43*, 1204.
(13) Zhou, G.; Parikh, S.; Tyler, P.; Evans, G.; Furneaux, R.; Zubkova, O.; Benjes, P.; Schramm, V. *J. Am. Chem. Soc.* **2004**, *126*, 5690.
(14) Jorgensen, R.; Merrill, A. R.; Yates, S. P.; Marquez, V. E.; Schwan, A. L.; Boesen, T.; Andersen, G. R. *Nature* **2005**, *436*, 979.
(15) Jorgensen, R.; Wang, Y.; Visschedyk, D.; Merrill, A. R. *EMBO Rep.* **2008**, *9*, 802.

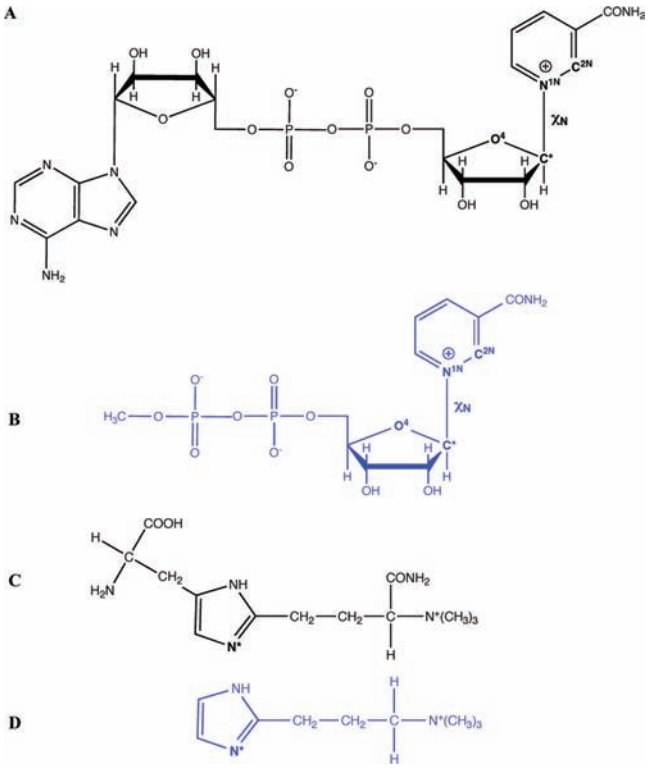

Figure 1. Chemical drawings of NAD^+ (A), NAD^+ model compound (B), diphthamide (C), and diphthamide model compound (D).

incoming nucleophile (water, cysteine, arginine, acetyl-lysine, or diphthamide) is covalently attached to the anomeric ADP-ribose C*, forming the respective product. This type of mechanism has been proposed for both nonenzymatic NAD^+ hydrolysis in water[16−18] and NAD^+ hydrolysis catalyzed by enzymes such as glycohydrolases[16,18,19] and pertussis toxin.[20,21] It has also been proposed for ADP-ribosylation of eukaryotic elongation factor 2 catalyzed by diphtheria toxin (DT)[12] and exotoxin A.[11,14,22,23] Central to the S_N1 reaction pathway is the question regarding stabilization of the oxocarbocation intermediate. Several hypotheses have been put forth. Oppenheimer and co-workers[17,18] studied the alkaline hydrolysis of NAD^+ and inferred that the source of stabilization of the oxocarbocation at high pH (>12.5) is ionization of the ribose diol: Creating a negative charge on the diol moiety by deprotonating one of the ribose −OH groups stabilizes the oxocarbocation intermediate. Although this mechanism is not directly applicable to reactions at ambient pH, the notion that a negative charge could stabilize the oxocarbocation has important implications for the enzyme-catalyzed NAD^+ hydrolysis. Indeed, in the family of ADP-ribosylating toxins, a highly conserved Glu is seen hydrogen bonded to the *N*-ribose 2′-OH group of NAD^+ in the X-ray structures. The glutamate's negative charge is thought to provide inductive stabilization of the oxocarbocation intermediate during the predominantly S_N1 reaction.[18,24]

In contrast to the S_N1 pathway, the S_N2 pathway involves concerted binding of the incoming nucleophile and departure of the leaving group (Scheme 2). This pathway has been postulated for NAD^+ hydrolysis in the absence of enzyme[19,25] and in the presence of enzymes such as sirtuins,[26,27] poly(ADP-ribose) polymerase,[28] as well as diphtheria, cholera, and pertussis toxins.[29] It has also been postulated for ADP-ribosylation of recombinant $G_{i\alpha1}$ subunits catalyzed by pertussis toxin.[21] That an oxocarbocation intermediate could not exist as a free solvent-equilibrated species was inferred from studies on the hydrolysis of acetophenone dimethyl ketals, whose results were extrapolated to a series of glycosides (base + sugar; no phosphate) and aliphatic acetals.[30] The estimated lifetime of a putative glycoside oxocarbocation was found to be quite short ($\sim10^{-12}$ s), so both the leaving group and the incoming nucleophile were thought to participate, although weakly and from a long distance, in stabilizing the glycoside oxocarbocation.[30] Indeed, a significant departure from the classical S_N2 mechanism has been reported in most studies, as the respective transition states appear to be quite "exploded" (dissociative) with significant oxocarbocation-like character.[21,25,27−29,31] For example, the TS structure for the nonenzymatic NAD^+ hydrolysis based on measured kinetic isotope effects (KIE) has highly oxocarbenium ion-like character where the nicotinamide N^{1N} and water oxygen are 2.65 and 3.00 Å from the reaction center C*, respectively.[25] Thus, NAD^+ hydrolysis in aqueous solution appears to proceed along a mixed "dissociative S_N2" pathway.

In studying the mechanism of NAD^+ C*−N^{1N} bond cleavage, the structure and properties of the nicotinamide-ribose fragment have been extensively studied. Factors such as changes in the bond distance, bond order, ionization of the ribose diol, rehybridization of anomeric carbon from sp^3 to sp^2, and hyperconjugation of the ribose ring have been taken into account in analyzing both experimental and theoretical data.[12,17,20,21,25,27−29,31,32] Strangely, the role of the NAD^+ diphosphate group (a flexible, doubly negatively charged, chemically reactive moiety) in the reaction process has largely been neglected. Notably, in many studies, NAD^+ with a net charge of −1 was modeled either as a nicotinamide ribonucleoside, lacking the pyrophosphate moiety with a net charge of +1,[12,31−33] or as a neutral nicotinamide mononucleotide with the dianionic pyrophosphate entity represented by a monoanionic phosphate group.[21,25,29] Thus, the effect of the NAD^+ overall −1 charge on the reaction process and the possibility of intra- and intermolecular interactions in the ground state and TS, especially involving the pyrophosphate, have not been explored. Furthermore, the role of other factors such as the type and nucleophilicity of the

(16) Bull, H. G.; Ferraz, J. P.; Cordes, E. H.; Ribbi, A.; Apitz-Castro, R. *J. Biol. Chem.* **1978**, *253*, 5186.
(17) Johnson, R. W.; Marschner, T. M.; Oppenheimer, N. J. *J. Am. Chem. Soc.* **1988**, *110*, 2257.
(18) Oppenheimer, N. J. *Mol. Cell. Biochem.* **1994**, *138*, 245.
(19) Tarnus, C.; Muller, H. M.; Schuber, F. *Bioorg. Chem.* **1988**, *16*, 38.
(20) Scheuring, J.; Schramm, V. L. *Biochemistry* **1997**, *36*, 4526.
(21) Scheuring, J.; Berti, P. J.; Schramm, V. L. *Biochemistry* **1998**, *37*, 2748.
(22) Yates, S. P.; Jorgensen, R.; Andersen, G. R.; Merrill, A. R. *Trends Biochem. Sci.* **2006**, *31*, 123.
(23) Armstrong, S.; Yates, S. P.; Merrill, A. R. *J. Biol. Chem.* **2002**, *277*, 46669.
(24) Holbourn, K. P.; Shone, C. C.; Acharya, K. R. *FEBS J.* **2006**, *273*, 4579.
(25) Berti, P. J.; Schramm, V. L. *J. Am. Chem. Soc.* **1997**, *119*, 12069.
(26) Smith, B. C.; Denu, J. M. *J. Am. Chem. Soc.* **2007**, *129*, 5802.
(27) Hu, P.; Wang, S.; Zhang, Y. *J. Am. Chem. Soc.* **2008**, *130*, 16721.
(28) Bellocchi, D.; Costantino, G.; Pellicciari, R.; Re, N.; Marrone, A.; Coletti, C. *Chem. Med. Chem.* **2006**, *1*, 533.
(29) Berti, P. J.; Blanke, S. R.; Schramm, V. L. *J. Am. Chem. Soc.* **1997a**, *119*, 12079.
(30) Young, P. R.; Jencks, W. P. *J. Am. Chem. Soc.* **1977**, *99*, 8238.
(31) Rising, K. A.; Schramm, V. L. *J. Am. Chem. Soc.* **1997**, *119*, 27.
(32) Schroder, S.; Buckley, N.; Oppenheimer, N. J.; Kollman, P. A. *J. Am. Chem. Soc.* **1992**, *114*, 8232.
(33) Scheuring, J.; Schramm, V. L. *Biochemistry* **1997**, *36*, 8215.

Scheme 1. S_N1 Mechanism

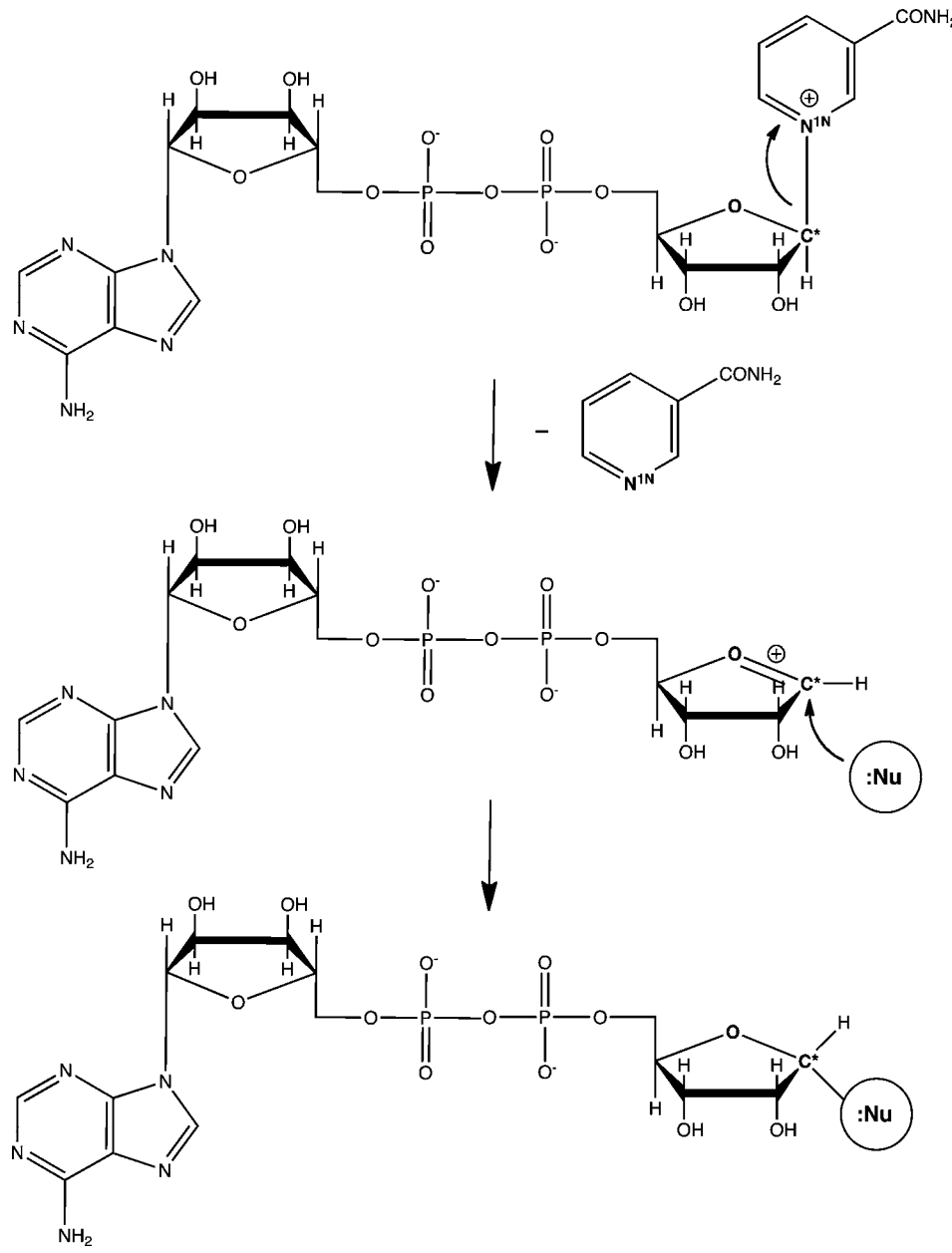

attacking molecule as well as the dielectric properties of the medium in influencing the reaction pathway have not been systematically evaluated.

In this study, we endeavor to fill in the aforementioned gaps in our current knowledge and elucidate the role of different internal and external factors in controlling the NAD$^+$ C*−N^{1N} bond cleavage. Using density functional theory combined with continuum dielectric methods, we modeled both S_N1 and S_N2 reaction pathways and systematically assessed (1) the role of the diphosphate group in stabilizing the NAD$^+$ ground state, oxocarbocation intermediate, reaction product, and nucleophile, (2) the chemical nature of the attacking nucleophile, and (3) the role of the protein matrix. Note that we do not assess these factors for a particular enzyme because our aim is not to determine the reaction mechanism of a particular enzyme, but to delineate the key determinants controlling the reaction pathway. The results reveal an intricate interplay between different factors in controlling the reaction pathway.

Methods

Models Used. NAD$^+$ (Figure 1A) was modeled as a methylated nicotinamide nucleotide diphosphate by substituting the adenosine moiety with a methyl group (Figure 1B). The overall charge of both NAD$^+$ and its model is the same, that is, −1. Diphthamide, which is a modified histidine (Figure 1C) found in eukaryotic elongation factor 2, was modeled as shown in Figure 1D. The nucleophilic N is marked with an asterisk.

Gas-Phase Calculations. Calculations were performed at the B3-LYP/6-31+G** level of theory using the Gaussian 03 program.[34] The B3-LYP/6-31+G** method has been employed in QM and QM/MM studies of NAD$^+$ ADP-ribosylation and has proven to successfully reproduce the basic features (geometries and

(34) Frisch, M. J.; et al. *Gaussian 03*; Gaussian, Inc.: Pittsburgh, PA, 2003.

Scheme 2. S_N2 Mechanism

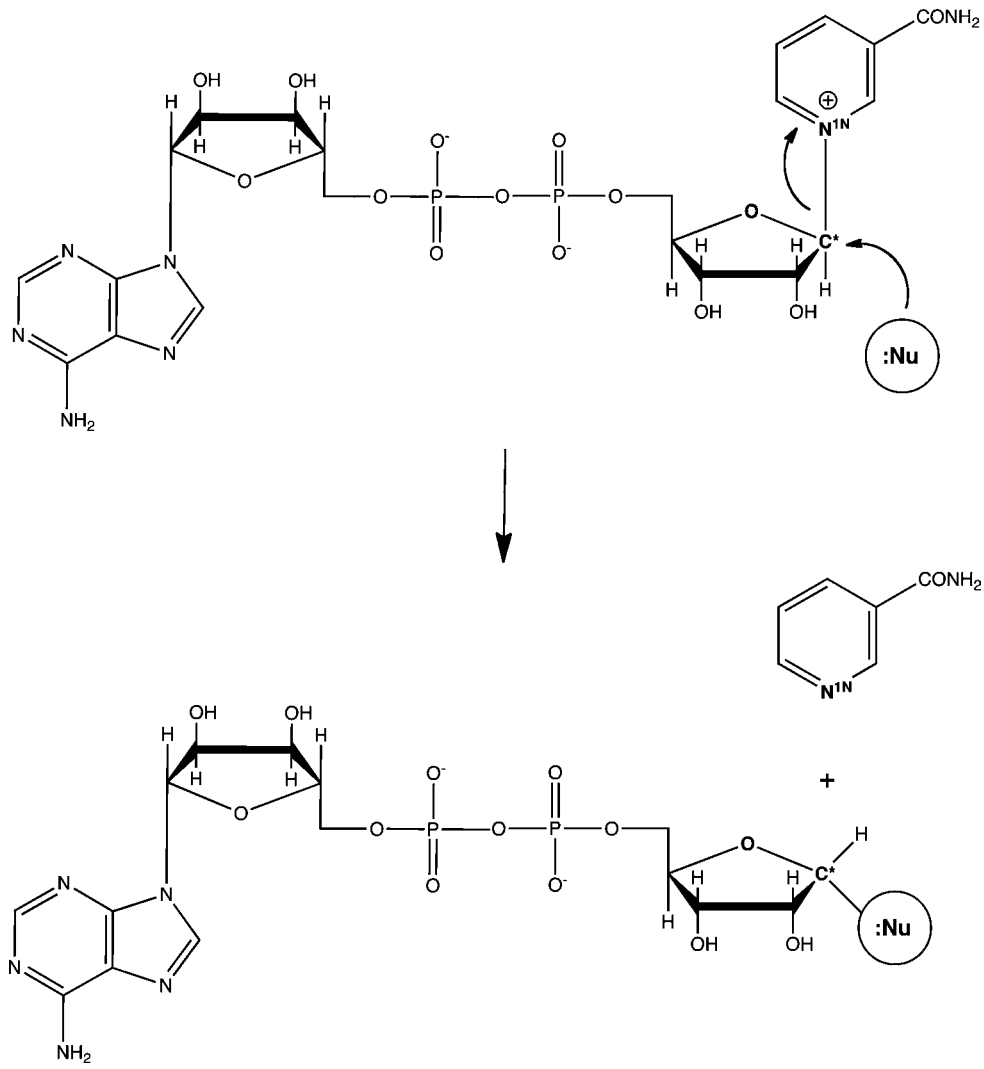

activation free energies) of the systems studied.[27,28] Herein, it was further calibrated against pertinent experimental data by using it to compute the gas-phase dissociation energies of charged labile A^+-B (A = H, K; B = C, N, O) bonds, resembling the charged N^+-C^* bond in NAD^+. The B3-LYP/6-31+G** method was found to reproduce the experimental gas-phase dissociation enthalpies of the charged A^+-B bonds in Table 1S (Supporting Information) to within 1 kcal/mol.

In modeling the first step of the S_N1 reaction (self-detachment of nicotinamide from the ribose ring), the C^*-N^{1N} bond was gradually elongated from its initial optimized value of 1.5 to 3.5 Å in 0.1 Å increments. The stretched C^*-N^{1N} distance was fixed during geometry optimization, while all the other internal coordinates were allowed to relax. At each fixed C^*-N^{1N}, the electronic energy relative to that of the fully optimized NAD^+ model, ΔE^1, was evaluated. Because the experimental activation entropy for the nonenzymatic S_N1 hydrolysis of NAD^+ ($T\Delta S^{\ddagger} = -0.16$ kcal/mol at 298 K) has been found to be negligible with respect to the activation energy (26.9 kcal/mol),[19] the entropic contributions to ΔE^1 were not considered in the present calculations.

In modeling the bimolecular S_N2 reaction, three types of nucleophiles differing in charge and nucleophilicity, water, hydroxide, and diphthamide, were used. The distance between the anomeric C* in NAD^+ and the attacking atom of the nucleophile (O* for water and hydroxide or N* for diphthamide) was chosen as the reaction coordinate. It was gradually reduced from 2.6 to 1.7 Å in 0.1 Å increment and kept frozen at each step, while all the other parameters were optimized. For a given reaction coordinate, the electronic energy relative to that of the two reactants at infinite separation, ΔE^1, was computed. Structures corresponding to the peak of the ΔE^1 plots as a function of the reaction coordinate were chosen for subsequent TS optimization. The TS species, representing first-order saddle points on the potential energy surface, were confirmed by a vibrational frequency analysis: A single imaginary frequency, resulting from the atomic displacements of the bond-forming and bond-breaking entities, was detected for each transition structure.

Condensed-Phase Calculations. The free energy for transferring a molecule in the gas phase to a medium characterized by dielectric constant $\varepsilon = x$, $\Delta G_{solv}{}^x$, was estimated by solving Poisson's equation using finite difference methods[35,36] with the MEAD (Macroscopic Electrostatics with Atomic Detail) program,[37] as described in previous works.[38] The effective solute radii were obtained by adjusting the CHARMM (version 22)[39] van der Waals radii to reproduce the experimental hydration free energies of model molecules containing the same type of functional groups as NAD^+

(35) Gilson, M. K.; Honig, B. *Proteins: Struct., Funct., Genet.* **1988**, *4*, 7.
(36) Lim, C.; Bashford, D.; Karplus, M. *J. Phys. Chem.* **1991**, *95*, 5610.
(37) Bashford, D. In *Scientific Computing in Object-Oriented Parallel Environments*; Ishikawa, Y., Oldehoeft, R. R., Reynders, V. W., Tholburn, M., Eds.; Springer: Berlin, 1997; Vol. 1343, p 233.
(38) Dudev, T.; Lim, C. *J. Am. Chem. Soc.* **2006**, *128*, 1553.
(39) Brooks, B. R.; Bruccoleri, R. E.; Olafson, B. D.; States, D. J.; Swaminathan, S.; Karplus, M. *J. Comput. Chem.* **1983**, *4*, 187.

and the nucleophiles to within 1 kcal/mol (see Supporting Information, Table 2S). The resulting values (in Å) are: $R_C = 1.95$, $R_N = 1.70$, $R_P = 2.10$, $R_H = 1.50$, $R_O(H_2O;O-C) = 1.88$, $R_O(O=C) = 1.80$, $R_O(O-P) = 1.56$, $R_O(OH^-) = 1.65$. The reaction free energy for a given environment characterized by a dielectric constant x is given by

$$\Delta G^x = \Delta E^1 - \Delta G^x_{solv}(\text{reactants}) + \Delta G^x_{solv}(\text{products}) \quad (1)$$

Results

NAD$^+$ in the Ground State. Rotation of the nicotinamide ring around the C*−N^{1N} bond results in different NAD$^+$ conformers, whose structures and overall energies vary with the strength of the intramolecular interactions. The 3D structures of NAD$^+$ bound to enzymes that catalyze the C*−N^{1N} bond cleavage exhibit a wide range of the O^4−C*−N^{1N}−C^{2N} (χ_N) dihedral angle ranging from 0.5° to ∼164° (Figure 1B). Most toxin-bound NAD$^+$ molecules have χ_N ranging from −8° to 10°, whereas sirtuin-bound NAD$^+$ has a χ_N of 165° (see Table 3S in the Supporting Information). Hence, various syn and trans conformers corresponding to the lower and upper ends of the observed χ_N angles, which capture the two extremities in the strength of intramolecular interactions, were fully optimized. Among the various optimized structures for the syn and trans conformers, a syn conformer **2a** with $\chi_N = -7.8°$ (Figure 2A) and a trans conformer **2b** with $\chi_N = 169°$ (Figure 2B) appear to be the most stable conformers where the diphosphate moiety exists in an extended conformation, as observed in the PDB structures. The distance between C* and the second (more distant) phosphorus P^A atom, which is a measure of the molecule's extent, for **2a** (6.8 Å) or **2b** (6.5 Å) is close to that for the respective NAD$^+$ conformer with a mean χ_N of −7.8° (PDB entries 3b8h-D and 3b78-F, C*−P^A = 7.1 Å) or 165° (PDB entry 2h4f, C*−P^A = 6.6 Å). Other syn and trans optimized structures were unrealistically compact, although some of them have energies lower than those of **2a** or **2b**. However, the latter have folded structures with C*−P^A distances (4.9−5.3 Å) significantly shorter than the X-ray values (see Table 3S), and hence they were not used for further evaluations. Because the pyrophosphate forms stronger H bonds with the nicotinamide amide in **2a** than with the pyridine C−H bonds in **2b**, it is not surprising that **2a** is more stable (by 10−13 kcal/mol) than **2b** in the gas phase and in water.

S$_N$1 NAD$^+$ Hydrolysis. To evaluate how the different NAD$^+$ conformations affect C*−N^{1N} bond cleavage, the free energies as a function of the C*−N^{1N} distance in **2a** and **2b** in the gas phase ($\Delta G^1 \approx \Delta E^1$) and in aqueous solution (ΔG^{80}) were computed. The resulting free energy profiles for **2a** (Figure 2A) and **2b** (Figure 2B) are quite different, indicating that the NAD$^+$ conformation does affect the C*−N^{1N} bond cleavage pathway: The results obtained (see below) imply that if the pyrophosphate group is not engaged in strong intra- or intermolecular interactions with other functional groups in the ground state or during the reaction, it can serve as an efficient intramolecular source of stabilization for the oxocarbocation intermediate.

Free Energy Profile of the Syn NAD$^+$ Conformer. When the pyrophosphate group forms strong O···H−N hydrogen bonds with the nicotinamide amide in **2a**, the gas-phase energy of **2a** keeps increasing with increasing C*−N^{1N} distance (Figure 2A, dashed black curve). That the energy does not decrease even after the C*−N^{1N} bond is cleaved implies a lack of stabilization of the resultant oxocarbocation. Indeed, the structures of the constrained optimized transient species (**2a′** and **2a″**) show that the positive charge developed on the ribose ring cannot be stabilized by intramolecular interactions with the diphosphate moiety, which is immobilized by strong H bonds to the −CONH$_2$ group of the departing nicotinamide. In aqueous solution, the free energy also does not decrease even after the C*−N^{1N} bond is broken (Figure 2A, solid blue curve). Hence, solvation does not suffice to stabilize the intermediate.

Free Energy Profile of the Trans NAD$^+$ Conformer. In contrast to **2a**, when the pyrophosphate group forms relatively weak O···H−C hydrogen bonds with the nicotinamide ring in **2b**, both the gas-phase and the solution free energy profiles of the less stable **2b** conformer exhibit a peak at C*−N^{1N} around 2.7−2.9 Å and a shoulder from C*−N^{1N} = 3.1−3.3 Å before descending steeply (Figure 2B). Analysis of the transient structures reveals that the positive charge developed on the ribose ring is stabilized by intramolecular interactions with the pyrophosphate, which is free to optimize its position and interactions in response to structural and electrostatic changes in the neighboring ribose moiety. As the positive charge on the anomeric C* ribose atom increases from 0.25e in **2b** to 0.48e when the C*−N^{1N} distance is 3.1−3.3 Å, the pyrophosphate group changes its geometry to enable one of its phosphates to hydrogen bond to the ribose 3′−OH group (structure **2b′**). This provides inductive stabilization of the oxocarbocation intermediate, which accounts for the shoulder in Figure 2B. This mechanism of intermediate species stabilization resembles the one invoked for oxocarbocation stabilization in toxins, which is achieved through intermolecular (as opposed to intramolecular) H-bonds between a conserved catalytic glutamate of the toxin and an −OH group of the *N*-ribose ring (see Introduction). As the C*−N^{1N} distance becomes ≥3.5 Å, the diphosphate group acquires more conformational freedom, and another means of stabilizing the oxocarbocation arises: The diphosphate group may act as an intramolecular nucleophile and form a chemical bond with the ribose C* atom. The resulting structure (**2b″**) is energetically more stable than **2b′** and accounts for the steep descent of the reaction energy when C*−N^{1N} is ≥3.5 Å (Figure 2B). Nearly the same **2b″** structure with a covalent pyrophosphate−ribose bond was obtained (figure not shown) when the nicotinamide was removed and the oxocarbocation intermediate was fully optimized (mimicking infinite separation between the two molecular entities).

To ensure that the above findings are not artifacts resulting from the model used, we repeated the calculations with the complete ADP molecule, where the adenosine moiety is attached to the pyrophosphate. As shown in Figure 3, the bulky and heavy adenosine substituent does not prevent the pyrophosphate group from making favorable contacts with the ribose ring and stabilizing the ADP-ribose intermediate (structure **3b**). The intermediate **3b** was verified to be a stable local minimum on the potential energy surface, as the vibrational frequencies are all positive.

S$_N$2 Water-Assisted NAD$^+$ Hydrolysis. The free energies as a function of the O^{water}−C* distance in **2a** and **2b** in the gas phase and in aqueous solution were also computed assuming a S$_N$2 pathway using water as the nucleophile. Unlike their S$_N$1 counterparts (Figure 2), the resulting free energy profiles for **2a** (Figure 4A) and **2b** (Figure 4B) are qualitatively similar: As the O^{water}−C* distance decreases from infinity to ∼2 Å, the energy of the system gradually increases. This is accompanied by an elongation of the C*−N^{1N} bond from its equilibrium value of 1.52 to ∼1.75 Å, which eventually breaks when the O^{water}−C*

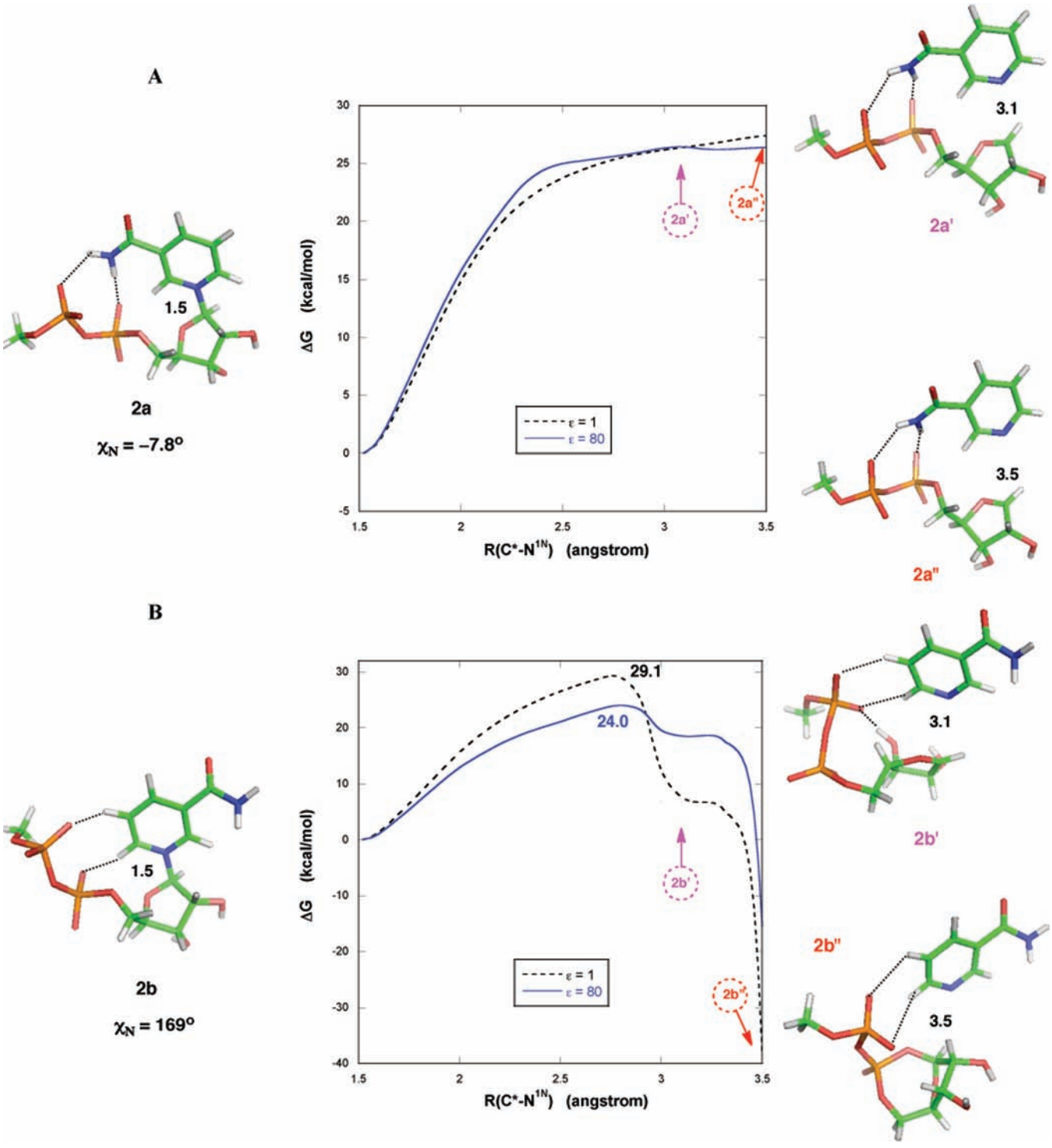

Figure 2. S_N1 reaction profiles for C*−N^{1N} bond cleavage of NAD^+ conformer **2a** (A) and **2b** (B) in the gas phase (black dashed curve) and in aqueous solution (blue solid curve) with reaction barriers in kcal/mol. Fully optimized ground-state structures with the C*−N^{1N} bond distances = 1.5 Å are shown on the left, while transient structures with the nicotinamide ring separated from the ribose moiety by 3.1 and 3.5 Å are shown on the right. Hydrogen bonds are denoted by black dotted lines.

distance is ≤2 Å. The pyrophosphate assists formation of the C*−OH bond by deprotonating the water; that is, a water H is transferred to a phosphate O. This accounts for the sharp decrease in the free energies when the O^{water}−C* distance is ≤2 Å. The S_N2 TS structures (**2a**+H_2O-TS and **2b**+H_2O-TS) corresponding to the **2a** and **2b** conformers have similar features: They are dissociative in character with the leaving nicotinamide N^{1N} and attacking water O* positioned at 2.7−2.8 Å from the C* reaction center. The pyrophosphate group preserves its extended conformation and contacts with the nicotinamide moiety found in the **2a** and **2b** ground states (see Figure 2). Note that the diphosphate group in both **2a** and **2b** stabilizes the S_N2 reaction product, whereas that in **2a** could not stabilize the S_N1 reaction product (see Figure 2A).

Quantitatively, the barrier height for **2b** (Figure 4B) is lower than that for **2a** (Figure 4A) in both the gas phase (by 5 kcal/

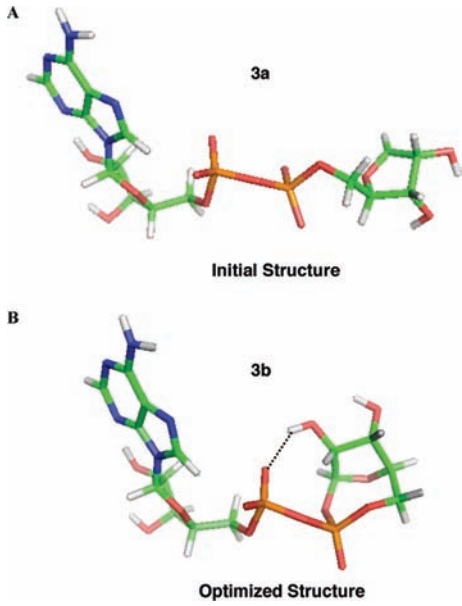

Figure 3. Initial (A) and B3LYP/6-31+G** fully optimized (B) structures of the ADP-ribose intermediate.

mol) and in aqueous solution (by 3.5 kcal/mol). This is probably due to the weaker intramolecular interactions in **2b** relative to **2a** (see above), which makes stretching of the C*−N^{1N} bond in **2b** less strained and hence less energy demanding than that in **2a**. Another difference is the presence of a shoulder in the **2a** profile (see Figure 4A, left) that is absent in the **2b** profile. This is probably because the pyrophosphate has stronger intramolecular interactions with the nicotinamide in **2a**, which limits its flexibility and retards its ability to position itself to receive the water proton. Note that for the **2b** conformer, the barrier height for the S_N2 reaction in aqueous solution (22.9 kcal/mol; Figure 4B) is slightly smaller than that for the S_N1 process (24.0 kcal/mol; Figure 2B).

S_N2 Hydroxide-Assisted NAD$^+$ Hydrolysis. The S_N2 reaction profiles for the hydroxide-assisted ADP-ribosylation of the model NAD$^+$ (conformer **2a**) in different dielectric media (Figure 5) show that the reaction proceeds more readily with a negatively charged nucleophile (OH^-) than with a neutral one (water). In the gas phase, the reaction proceeds without a barrier, as the gas-phase energies are all very negative due to strong attractive interactions between the electronegative hydroxide O and the electropositive ribose C*. In contrast to the dissociative transition states found for the water-assisted NAD$^+$ hydrolysis, the TS structure (**2a**+OH-TS) is an "early" reactant-like complex with the hydroxide O and nicotinamide N^{1N} located at 2.75 and 2.33 Å from C*, respectively. In a buried active site characterized by $\varepsilon = 4$, the reaction also proceeds without a barrier, as the desolvation penalty of the reactants is largely compensated by favorable solvation of the dianionic product complex. However, in water, the reaction proceeds with a barrier of 5.8 kcal/mol.

S_N2 Diphthamide Attack of NAD$^+$. Diphthamide uses its nucleophilic nitrogen from the imidazole ring (N* in Figure 1C,D) for ADP-ribosylation. However, it is expected to interact differently with NAD$^+$ depending on the orientation of its cationic $-N^+(CH_3)_3$ "tail" relative to the anionic pyrophosphate. Accordingly, in modeling the S_N2 reaction pathway, two types of reactant structures were fully optimized (see Figure 6): one with the diphthamide "tail" positioned alongside the pyrophosphate moiety and engaged in strong electrostatic interactions with the phosphates (**6a**), and the other with the diphthamide "tail" oriented opposite the diphosphate group (**6b**). The S_N2 reaction profiles for these two structures in the gas phase ($\varepsilon = 1$), in a protein environment ($\varepsilon = 4$), and in water ($\varepsilon = 80$) are shown in Figure 6A and B, respectively.

Free Energy Profile for 6a. Because of strong favorable interactions between the oppositely charged diphthamide and pyrophosphate entities in **6a**, the gas-phase energies are negative despite the attack of a positively charged diphthamide at a positively charged ribose C* (Figure 6A). However, the high desolvation penalty for the two charged reactant species offset this energy gain so that there is a reaction barrier in a protein environment (5.0 kcal/mol), which becomes significantly larger in aqueous solution (31.2 kcal/mol). This brings out the importance of the protein matrix: Relative to aqueous solution, the lower dielectric environment of the protein matrix enhances the favorable interactions between the positively charged diphthamide and negatively charged pyrophosphate in **6a**, thus lowering the reaction barrier significantly. As in the water-assisted NAD$^+$ hydrolysis, the TS structure, **6a-TS**, in Figure 6 is dissociative, but with more pronounced product-like features (C*−N^{1N} > N*−C*).

Free Energy Profile for 6b. The less favorable interactions between the reactants in **6b** result in higher-energy reaction profiles (Figure 6B). Although the gas-phase reaction is still barrierless, the gas-phase energy as the diphthamide approaches the *N*-ribose in **6b** is significantly less favorable than that for **6a**. Likewise, the barriers for **6b** in a protein environment (38.8 kcal/mol) and in aqueous solution (52.5 kcal/mol) are much higher than those for **6a** (5.0 and 31.2 kcal/mol). Thus, although the nucleophilic group attacking **6a** and **6b** is the same (the imidazole "head"), a proper orientation of the diphthamide "tail" relative to the pyrophosphate group appears to be important in determining the reaction kinetics.

Free Energy Profile for Imidazole. The above finding becomes more evident when comparing the free energy profile for diphthamide attack of **6a** (Figure 6A) or **6b** (Figure 6B) with that for imidazole attack of NAD$^+$ (Figure 6C), that is, with only the diphthamide "head" but omitting its "tail". The barrier for the reaction of imidazole with NAD$^+$ in a protein environment (18.0 kcal/mol) is between that for the reaction of **6a** (5.0 kcal/mol) and **6b** (38.8 kcal/mol). The substantial energy differences between the reference imidazole and diphthamide nucleophiles appear to be associated with the presence and specific properties of the $-CH_2-CH_2-CH_2-N^+(CH_3)_3$ group attached to the imidazole ring. As compared to water-assisted NAD$^+$ hydrolysis (Figure 4), imidazole-assisted ADP-ribosylation has a lower reaction barrier in the gas phase (Figure 6C) due to the more favorable interactions of the ribose ring with imidazole, which has a larger dipole moment ($\mu^{calc} = 3.8$ D) and polarizability ($\alpha^{calc} = 46.4$ au^3) than water ($\mu^{calc} = 2.1$ D; $\alpha^{calc} = 7.0$ au^3).

Discussion

Because the bond between the *N*-ribose anomeric C* and the nicotinamide N^{1N} is cleaved during non-redox reactions involving NAD$^+$, previous works have focused on the structure and properties of the nicotinamide and ribose entities. Although the specific nature of their pairing determines to a large extent the molecule's behavior in aqueous solution and in a protein, this work reveals several other factors that can strongly influence and exert control on the reaction pathway. In particular, the

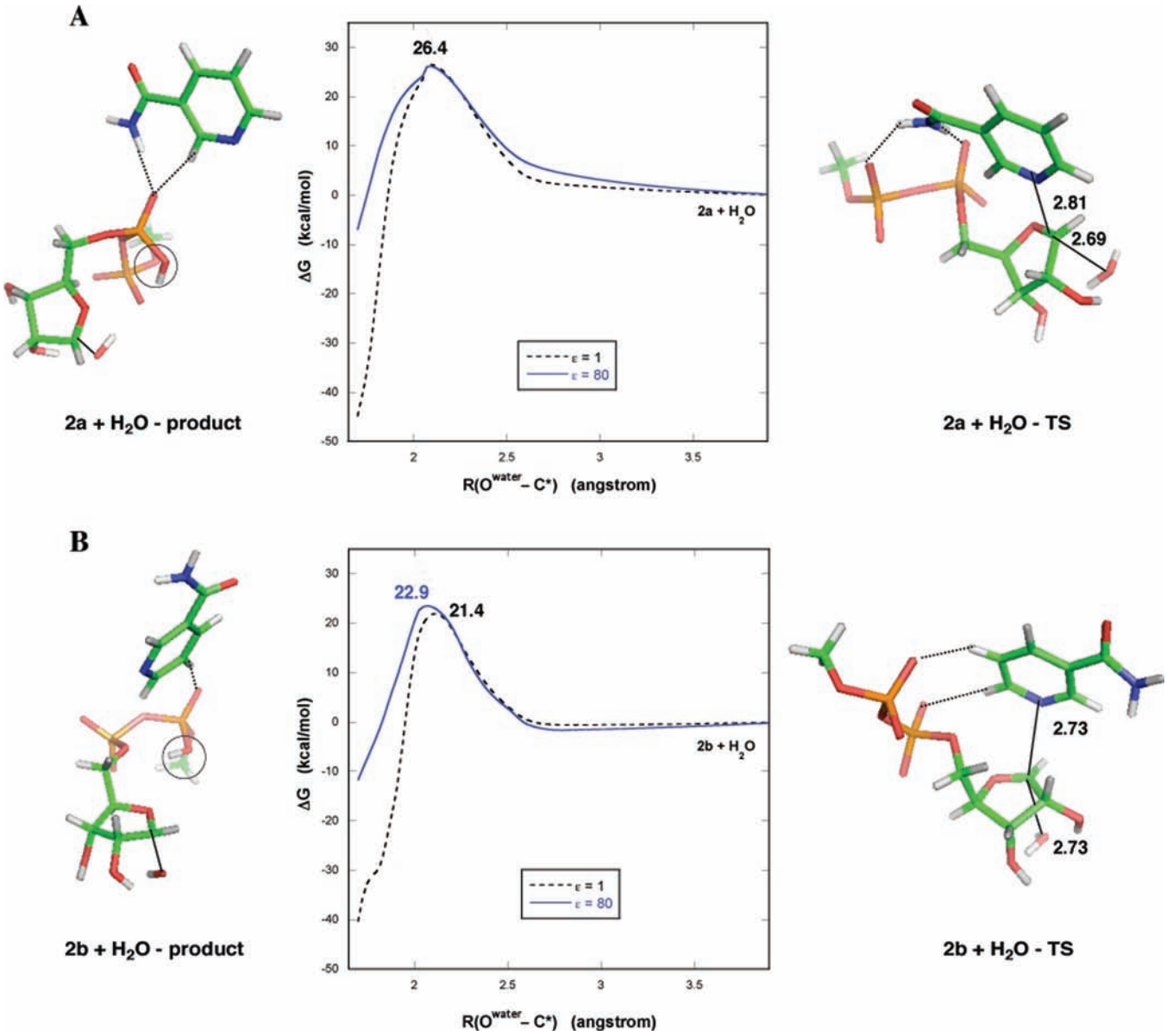

Figure 4. S_N2 reaction profiles for the water-assisted hydrolysis of NAD^+ conformer **2a** (A) and **2b** (B) in the gas phase (black dashed curve) and in aqueous solution (blue solid curve) with reaction barriers in kcal/mol. Transition state structures with bond distances in angstroms are shown on the right, while reaction products are depicted on the left. Hydrogen bonds are denoted by black dotted lines.

highly flexible, reactive, and charged pyrophosphate group, although not located in the immediate vicinity of the C* reaction center, is found to play an important role in non-redox reactions involving NAD^+. The findings are compared to available experimental data.

The Role of the Pyrophosphate Moiety. In Stabilizing the Oxocarbenium Intermediate. Our results show that the pyrophosphate group could efficiently stabilize the reaction intermediate of the unimolecular S_N1 reaction, thus facilitating the reaction (structures **2b′**, **2b″** in Figure 2B and **3b** in Figure 3). To achieve such stabilization, the diphosphate group should possess enough conformational freedom and be liberated of strong intra- or intermolecular contacts with other chemical groups from its surroundings in the ground state or during reaction. If immobilized, for example, by hydrogen bonds with the nicotinamide amide group (structures **2a**, **2a′**, and **2a″** in Figure 2A), it cannot orient itself to stabilize the developing positive charge on the ribose ring as the nicotinamide departs, thus disfavoring the S_N1 pathway (Figure 2A). In such a case, the S_N1 pathway may still occur if there is an external protein donor that could act analogous to the pyrophosphate group and provide inductive stabilization of the reaction intermediate.

In Stabilizing the Nucleophile. In addition to its role in the S_N1 reaction, the dianionic pyrophosphate can also affect the course of the bimolecular S_N2 reaction, especially when the attacking nucleophile is positively charged like diphthamide. The calculations show that attractive electrostatic interactions between the pyrophosphate and the $-CH_2-CH_2-CH_2-N^+(CH_3)_3$ group from diphthamide can significantly lower the reaction barrier (Figure 6A), whereas a lack of such interactions results in elevated reaction barriers (Figure 6B and C). This finding is consistent with experimental observations showing that ADP-ribosylation catalyzed by diphtheria toxin or exotoxin A (involving diphthamide attack of NAD^+) is much faster than the reaction catalyzed by the same enzyme in the absence of

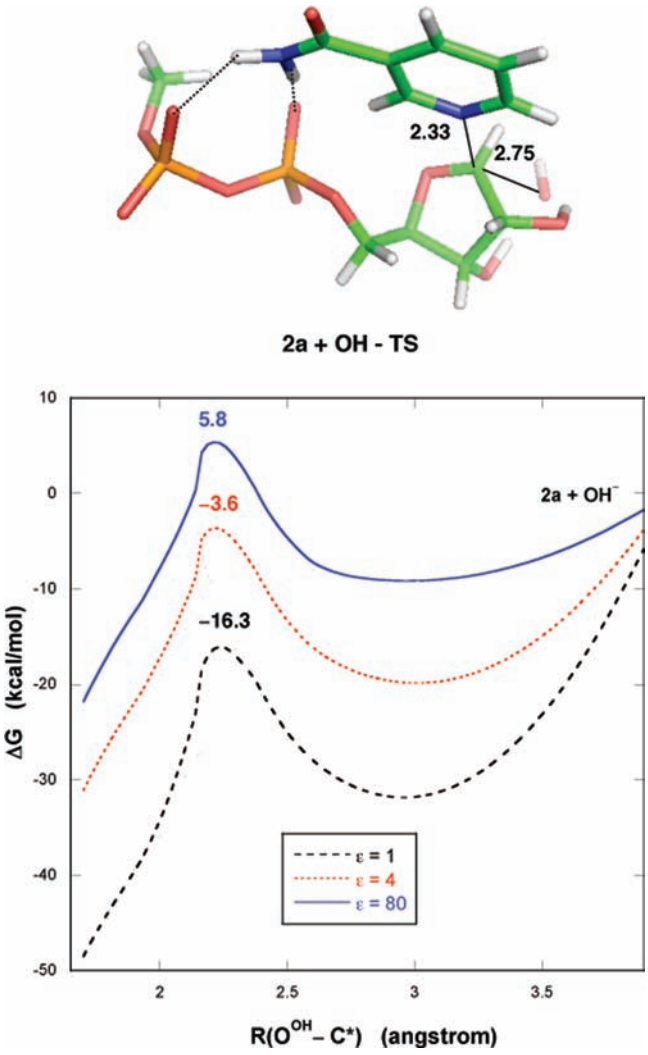

Figure 5. (Top) Transition state structure with bond distances in angstroms and hydrogen bonds denoted by black dotted lines. (Bottom) S_N2 reaction profiles for the hydroxyl-assisted ADP-ribosylation of NAD^+ conformer **2a** in the gas phase (black dashed curve), in a buried active site (red dotted curve), and in aqueous solution (blue solid curve) with reaction barriers in kcal/mol.

diphthamide.[22,40] It is also consistent with the TS model proposed for ADP-ribosylation catalyzed by exotoxin A, where the diphthamide trimethyl ammonium group is placed adjacent to the NAD^+ phosphates.[15]

In Stabilizing the Product. The pyrophosphate moiety can aid product formation by serving as a proton acceptor to deprotonate water in the final stages of the water-assisted S_N2 hydrolysis (**2a**+H_2O-product and **2b**+H_2O-product, Figure 4). Interestingly, it becomes activated to change its geometry and accept a proton only when the $O^{water}-C^*$ bond starts to form ($O^{water}-C^* \leq 1.8$ Å). The trigger appears to be the increase in positive charge of the water proton (that would be transferred to the pyrophosphate group), which is almost constant (0.52e) when $O^{water}-C^*$ decreases from 2.6 to 2.0 Å, but increases to 0.55−0.56e when the $O^{water}-C^*$ is ≤1.8 Å. At earlier stages of the S_N2 hydrolysis, the diphosphate moiety is inactive and retains its extended conformation (**2a**+H_2O-TS and **2b**+H_2O-TS).

The Role of the Attacking Nucleophile. For the three types of nucleophiles studied, the calculations reveal that the TS structures depend on the amount of negative charge of the attacking atom. The TS species formed by hydroxide, water, and diphthamide attack, which are all dissociative, change from "early" to "late" structures in line with decreasing partial negative charge on the respective nucleophilic atoms: the distance between the C* reaction center in **2a** and the attacking nucleophilic atom of OH^-, H_2O, and diphthamide is 2.75, 2.69, and 2.37 Å, respectively, while the NBO charges on the hydroxide O, water O, and diphthamide N are −1.40e, −0.99e, and −0.52e, respectively. This is because the greater is the charge on the attacking nucleophilic atom, the earlier (from longer distance) favorable electrostatic interactions with C* can occur, and hence the weaker is the bond to the stronger nucleophile.

The calculations also reveal how the reaction barrier depends on the nature of the nucleophile. Relative to water, the higher nucleophilicity of hydroxide results in stronger attractive interactions with the ribose C*, and thus no energy barrier for hydroxide attack in the gas phase or in a low dielectric medium (compare Figures 4 and 5). The orientation of the diphthamide $-CH_2-CH_2-CH_2-N^+(CH_3)_3$ tail may act as a controlling switch for the NAD^+ C^*-N^{1N} bond cleavage by altering the barrier: Maximizing its electrostatic interactions with the NAD^+ pyrophosphate group accelerates the reaction, whereas an unfavorable "tail" orientation slows the process.

The Role of the Dielectric Medium. The dielectric properties of the medium have opposite effects on the S_N1 and S_N2 reaction mechanisms. Increasing the dielectric constant of the medium reduces the barrier for the S_N1 reaction, but destabilizes the oxocarbocation intermediate so that the pathway becomes more S_N2-like (see Figure 2B). In contrast, it raises the barrier for the S_N2 pathway, regardless of the nucleophile (Figures 4B, 5, and 6). However, the extent to which solvent effects raise the barrier for the S_N2 pathway differs depending on the net charge of nucleophile: it is larger for S_N2 reactions involving charged nucleophiles such as hydroxide (Figure 5) and diphthamide (Figure 6A and B) than for reactions with neutral water (Figure 4) and imidazole (Figure 6C). Thus, by manipulating the solvent exposure of the NAD^+-binding site, the protein could control the reaction mechanism and rate (see below).

Implications/Significance. The exact mechanism (S_N1 or S_N2) requires compute-intensive QM/MM calculations in hand with experimental structural, thermodynamic, and kinetic data for the enzyme of interest. Our results, nevertheless, elucidate some key factors controlling the reaction pathway, which in turn suggests ways in which the enzyme can accelerate the reaction, as summarized below.

(1) An enzyme can accelerate the reaction of NAD^+ with water or diphthamide by excluding solvent from the active site upon binding NAD^+: decreasing the dielectric constant decreases the reaction barrier (see Figures 4B, 5, and 6). This finding is consistent with the observation in the crystal structure of NAD^+ bound to exotoxin A and eukaryotic elongation factor 2 that an exotoxin A loop interacts with NAD^+ to occlude solvent from the active site.[15]

(2) Because the effect of solvent exclusion from the enzyme's active site on the rate for reaction with a water molecule is not significant as compared to that for reaction with a charged nucleophile like OH^-, the enzyme could additionally accelerate NAD^+ hydrolysis by supplying a general base that could deprotonate the water nucleophile: the reaction with OH^- is predicted to proceed with negligible barrier in a buried active site (Figure 5). On the other hand, if the NAD^+-binding pocket

(40) Gill, D. M.; Pappenheimer, A. M. J.; Brown, R.; Kurnick, J. T. *J. Exp. Med.* **1969**, *129*, 1.

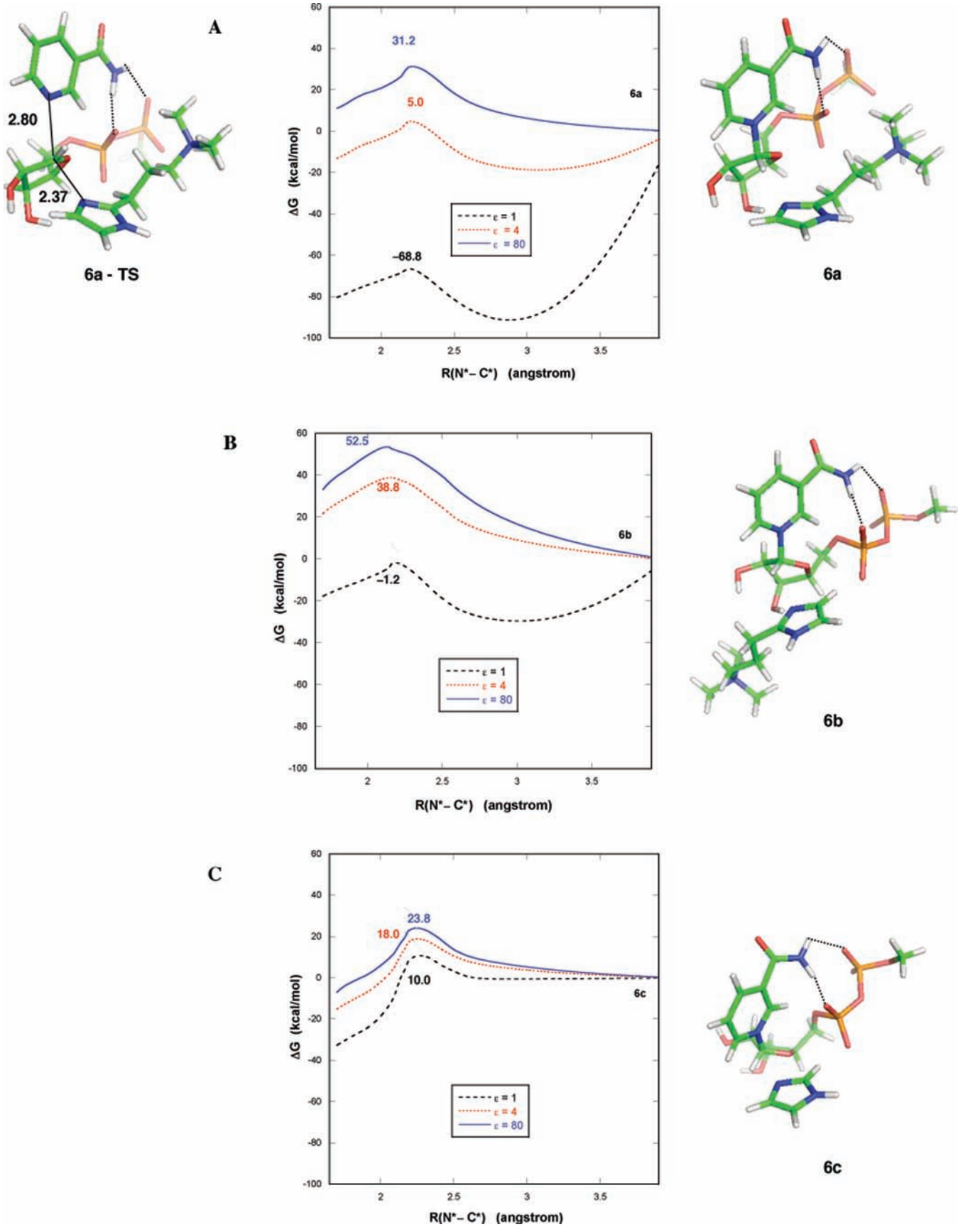

Figure 6. S_N2 reaction profiles for diphthamide-assisted ADP-ribosylation of NAD^+ conformer **2a** with the diphthamide "tail" besides the pyrophosphate group (A) and opposite the diphosphate moiety (B), and for imidazole-assisted ADP-ribosylation of NAD^+ conformer **2a** (C) in the gas phase (black dashed curve), in a buried active site (red dotted curve), and in aqueous solution (blue solid curve); reaction barriers are in kcal/mol. Reactant structures are shown on the right, while the TS structure for **6a** is depicted on the left with bond distances in angstroms and hydrogen bonds denoted by black dotted lines.

is relatively solvent exposed, the enzyme could catalyze NAD^+ hydrolysis by supplying an active site carboxylate, which can act in lieu of the pyrophosphate group to effectively stabilize the positive charge on the oxocarbocation TS/intermediate (see Figure 2B).

(3) An enzyme can accelerate the NAD^+ C*−N^{1N} bond cleavage by its interactions with the pyrophosphate moiety, which in turn dictates the freedom of the diphosphate group to interact with the oxocarbenium intermediate, the nucleophile, and/or the product (see above). Notably, enzymes such as DT and exotoxin A can catalyze the reaction of NAD^+ with diphthamide by not only providing a low dielectric environment for the reaction, but also an electrostatically favorable environment to attract the positively charged diphthamide moiety to the negatively charged NAD^+ phosphates. The favorable interactions between the oppositely charged trimethyl ammonium and pyrophosphate entities would help to lower the barrier for the approach of diphthamide to NAD^+ (see Figure 6A).

(4) In addition to the enzyme, another key factor controlling the reaction rate is the nucleophile itself: attacking agents with (a) high nucleophilicity like hydroxide or (b) a cationic group that can interact favorably with the NAD^+ diphosphate group like diphthamide yield lower reaction barriers.

(5) Our calculations do not support ground-state destabilization as a key factor in which the enzyme accelerates NAD^+ ADP-ribosylation. Ground-state destabilization had been postulated to explain the accelerated NAD^+ ADP-ribosylation by DT based on the unusually small χ_N angle (4°) of NAD^+ bound to DT (1tox) as compared to the much larger χ_N angles of NAD^+ bound to 23 oxidoreductase enzymes.[41] Whereas previous work assumed the small χ_N angle might strain the *N*-glycosidic bond, this work shows that the NAD^+ conformer with a small χ_N angle (**2a**) is in fact more stable than that with a large χ_N angle (**2b**) in the gas phase and in water. Furthermore, the more stable **2a** conformer yields a higher barrier for NAD^+ hydrolysis in water than the **2b** conformer for both S_N1 (Figure 2) and S_N2 pathways (Figure 4).

Acknowledgment. This work is supported by the Institute of Biomedical Sciences, Academia Sinica, and the NSC contract no. NSC 95-2113-M-001-001.

Supporting Information Available: Complete ref 34, Tables S1−S3, and *xyz* coordinates of fully optimized ground state, TS, and reaction products of conformers **2a** and **2b**. This material is available free of charge via the Internet at http://pubs.acs.org.

JA106600K

(41) Bell, C. E.; Yeates, T. O.; Eisenberg, D. *Protein Sci.* **1997**, *6*, 2084.